INFLUENCE OF BOUNDARY CONDITIONS ON OXYGEN DISTRIBUTION IN AN ORGAN-ON-A-CHIP PLATFORM

VIOLETA CARVALHO[1,2,3,*], NELSON RODRIGUES[2], RAQUEL O. RODRIGUES[3,4,6,7], MANUEL BAÑOBRE[6], RUI A. LIMA[1,5] AND SENHORINHA TEIXEIRA[2]

[1] MEtRICs, University of Minho, Guimarães, Portugal, violeta.carvalho@dps.uminho.pt; nrodrigues@dem.uminho.pt; rl@dem.uminho.pt;
[2] ALGORITMI research centre/LASI, University of Minho, Guimarães, Portugal, st@dps.uminho.pt
[3] Center for Microelectromechanical Systems (CMEMS-UMinho), University of Minho, Guimarães, Portugal, raquel.rodrigues@dei.uminho.pt
[4] LABBELS—Associate Laboratory, Braga/Guimarães, Portugal
[5] CEFT, Faculty of Engineering of the University of Porto (FEUP), Porto, Portugal
[6] Advanced (magnetic) Theranostic Nanostructures Lab, Nanomedicine Unit, INL–International Iberian Nanotechnology Laboratory, Av. Mestre José Veiga, Braga 4715-330, Portugal, manuel.banobre@inl.int
[7] Division of Engineering in Medicine, Brigham and Women's Hospital, Department of Medicine, Harvard Medical School, Cambridge, MA 02139, USA

Keywords: *CFD, Organ-on-a-chip, Fluid flow, Diffusion gradients, Microfluidics*

Abstract. Organ-on-a-chip (OoC) platforms have revolutionized the drug development process by offering an effective alternative to animal models. These advanced microfluidic platforms mimic the organ functions at a microscale, and they can be produced at a large scale and at a lower price. Despite the variety of OoC models developed up to now, the combination of numerical simulations with experimental procedures has been of paramount importance in the development of more realistic and effective OoC devices. In addition, a better understanding of the physical phenomena happening in OoC can be obtained.

In the present work, fluid flow numerical simulations were carried out in an OoC aiming to evaluate the influence of imposing different inlet velocities on the oxygen distribution along the device. This is of great importance to understand if the oxygen that reaches the cells is adequate for their culture. The results showed that for the geometry tested, with four organ models in parallel, by increasing the inlet velocity, the dissolved oxygen where cells are cultured also increases. This proves the importance of using numerical simulations for improving the performance of the experimental tests and optimizing the flow conditions.

1   INTRODUCTION

Over the years, numerical simulations have been increasingly used in biomedical research, namely in organ-on-a-chip - OoC technology [1,2]. OoC devices emerged to fill the gap between animal testing and two-dimensional *in vitro* models which are inadequate to mimic the physiology of the human organs [3,4]. Besides, OoCs have greatly contributed to the 3Rs principle, Refine, Reduce, and Replace [5]. By combining microfluidic technology with cell

culture, these devices have been applied to study alternative therapies for numerous diseases, such as cancer [6].
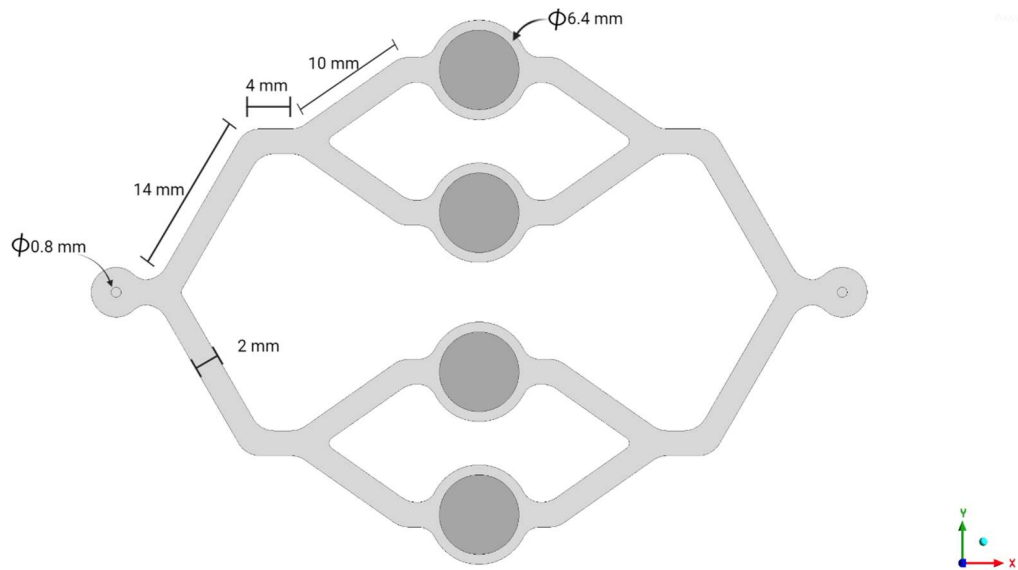
Cancer remains a critical disease around the world and affects people of all ages, which makes it particularly explored. Furthermore, given the adverse side effects of chemotherapy, researchers have focused their research on the development of targeted therapies through nanocarriers. Several studies can be found in the literature, however, the preclinical tests of these nanoformulations commonly fail which delays their approval by the regulatory entities. For this reason, the development of increasingly relevant *in vitro* models has been made in which numerical simulations are an important part [7–10]. The device geometry and experimental conditions can be improved, and insights about the fluid flow can be obtained [2,11]. For instance, Kocal and co-workers [12] used computational tools to understand the relationship between the fluid shear stress and the phenotypic changes of cancer cells along a cancer-on-a-chip device. Other researchers have modeled porous membranes to simulate the diffusion of elements important to cells such as oxygen and glucose [13,14]. Wong et al. [15] created a computational model in which cells are cultured on a porous membrane support and the device was adjusted to operate with physiological shear stresses, to facilitate the transport of secreted biomolecules. Chen et al. [16] developed a similar model and evaluated the influence of flow flux, wall shear stress, and transmembrane pressure difference on the chip geometry and membrane permeability. Other authors studied the influence of velocity fields on spheroids' growth [17]. The authors observed that when applying a lower velocity, the spheroid growth can be reduced due to the oxygen concentration downstream of the spheroid surface being not enough. In contrast, Bhise et al. [18] modeled organoids as a porous body and evaluated the oxygen consumption as well as the influence of using different velocities. Similarly, Yi et al [19] studied the consumption of oxygen on the organoids through numerical simulations.

Despite the advances made, for the numerical outcomes being accurate, the results have to be mesh independent, and the appropriate boundary conditions, fluid properties, and models selected have to be set. In this regard, in the present work, the influence of imposing different inlet velocities on the oxygen transport was numerically evaluated by using Ansys Fluent software [20].
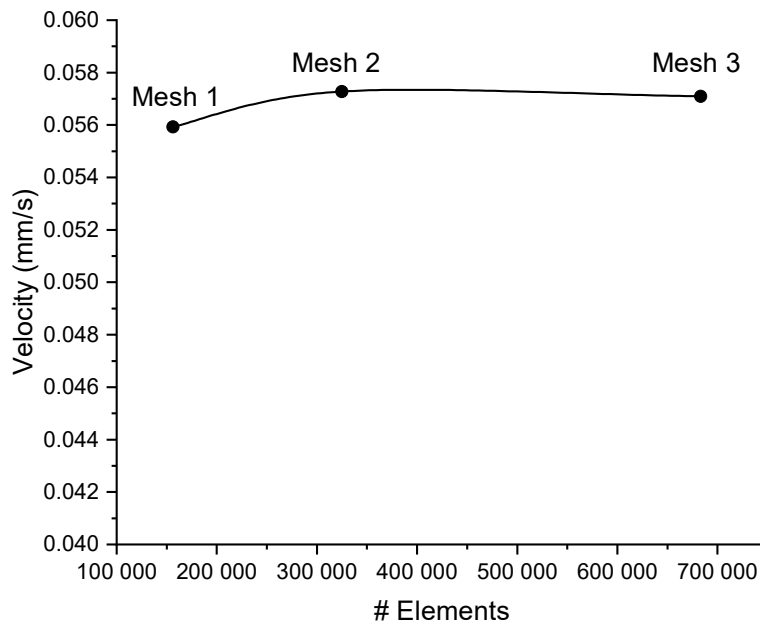
2 NUMERICAL MODELING

2.1 Geometry and Mesh

In Figure 1, the geometry and dimensions of the OoC developed are presented. As can be observed, the device divides into four branches in parallel. Note that the height of the device and the organoid are 5 mm and 2 mm, respectively.
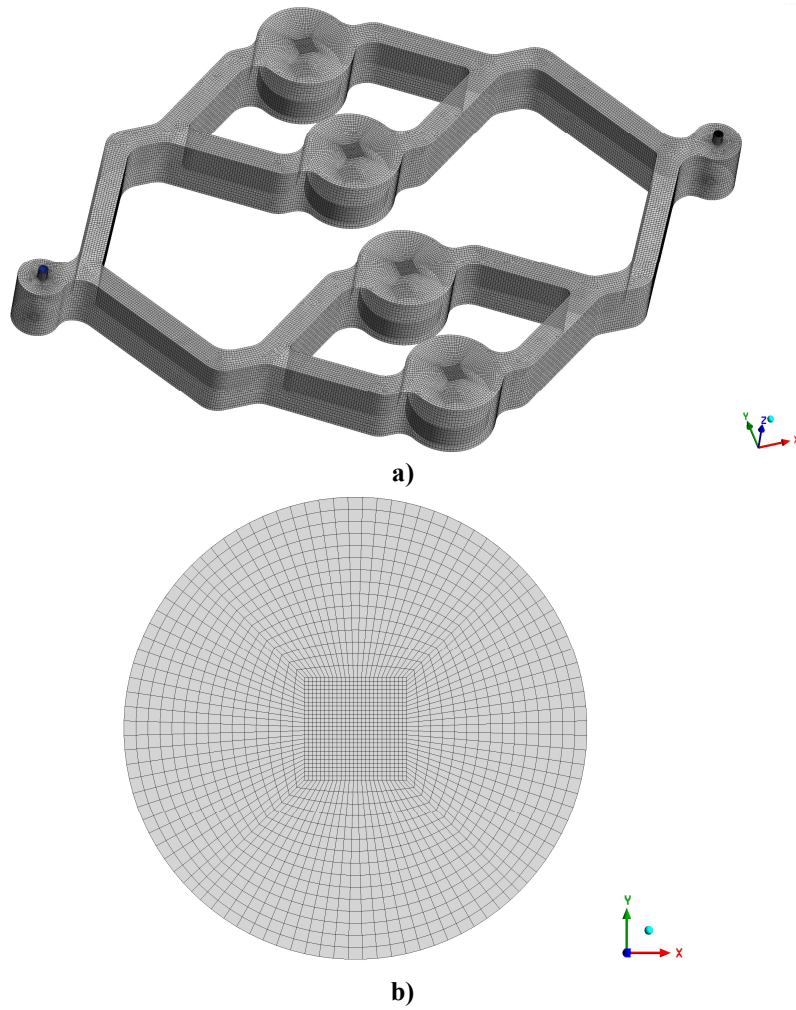
Figure 1. Geometry and dimensions of the OoC.

After the geometry definition, a mesh study was conducted to ensure that the results are mesh-independent. To this end, three structured hexahedral meshes were developed and the velocity was evaluated at one point at the center of the organoid since this is the region of interest. Figure 2 shows the velocity variation by increasing the number of mesh elements (Mesh 1 – 156,372; Mesh 2 – 325,068 and Mesh 3 – 683,370). By observing the results, it can be seen that between Mesh 2 and 3 the velocity is quite similar. Thus, Mesh 2 was selected to conduct the numerical simulations.

Figure 2. Velocity variation with mesh refinement.

The selected mesh is presented in Figure 3 a), and in Figure 3 b) the mesh in the organoids region was zoomed to better observe the mesh refinement.

3

a)

b)

Figure 3. a) Selected mesh to run the numerical simulations and b) Mesh in the organoid region.

2.2 Governing Equations

In the present work, the flow of culture medium through the OoC was simulated by using Ansys Fluent software. The fluid was assumed to be Newtonian and incompressible with a density of $1007 \, \text{kg/m}^3$, and a constant viscosity of $0.958 \times 10^{-3} \, \text{kg/(m} \cdot \text{s)}$ [21], and the flow was assumed to be laminar.

The flow of culture medium was governed by the Navier-Stokes equations for continuity (Equation 1) and momentum (Equation 2) as follows.

$$\nabla \cdot \vec{u} = 0 \tag{1}$$

$$\rho \left(\vec{u} \cdot \nabla \right) = -\nabla p + \mu \nabla^2 \vec{u} \tag{2}$$
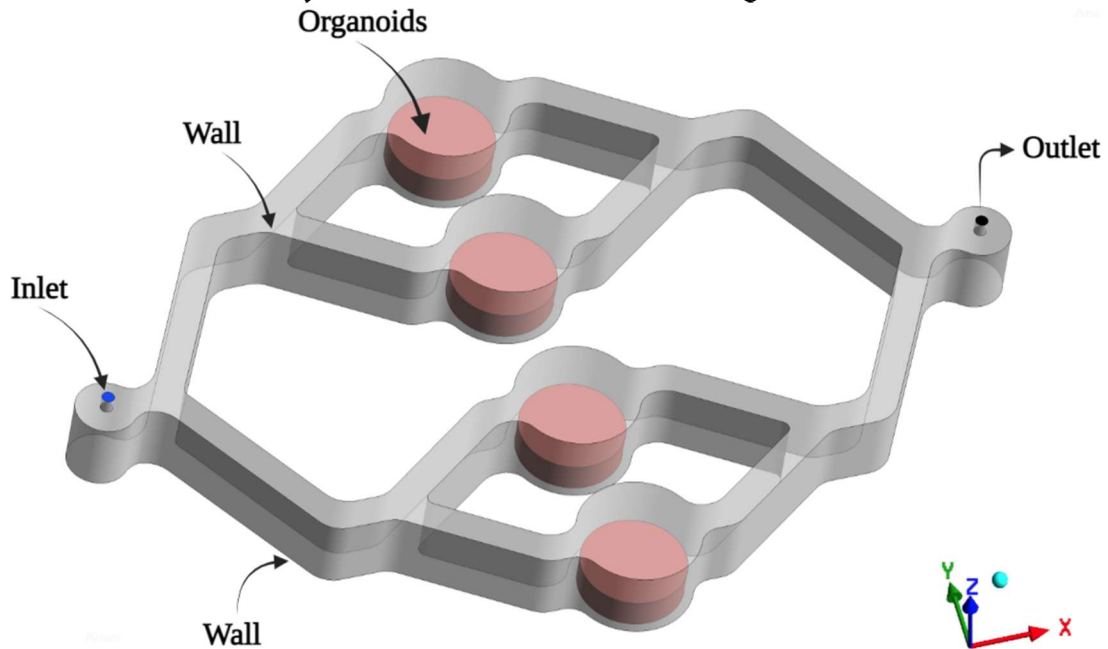
Regarding the oxygen transport, this was made considering the presence of a scalar. For steady-state simulations, Equation 3 will be solved [20]:

$$\frac{\partial}{\partial x_i}\left(\rho u_i \phi_k - \Gamma_k \frac{\partial \phi_k}{\partial x_i}\right) = S_{\phi_k} \quad k = 1, \ldots, N \quad (3)$$

where Γ_k and S_{ϕ_k} are the diffusion coefficient and source term for each of the N scalar equations.

2.3 Boundary Conditions

In order to evaluate the influence of the inlet velocity on the oxygen distribution, the velocity at the inlet was varied (2.32 mm/s, 3.98 mm/s, 11.14 mm/s, and 20 mm/s). A pressure outlet was defined at the outlet of the fluid, and the walls of the device were assumed to be rigid by applying a no-slip condition. Moreover, the oxygen concentration that reaches the outlet was imposed at the inlet, the oxygen consumption by cells was considered, and the oxygen diffusion in the organoid and the culture medium was distinguished, being 5×10^{-10} m^2/s and 2.7×10^{-9} m^2/s, respectively [22,23]. Note that, all simulations were run in a steady state. A schematic representation of the boundary conditions can be observed in Figure 4.

Figure 4. Boundary conditions considered to conduct the numerical simulations.

Furthermore, the oxygen entrance was assumed to be in the upper wall of the OoC. In order to set an oxygen concentration as close as possible to the experimental conditions, the dissolved oxygen in the OoC was measured. For this purpose, an Extech DO210 Dissolved Oxygen Meter was used. However, due to the equipment's technical specifications, for the measurements being accurate, water was used instead of the culture medium. For this reason, the experimental setup was prepared and water flowed inside the OoC for 24h without cells while maintained in the cell culture incubator as outlined in Figure 5. Three measurements were made, and the mean concentration was equal to 0.19 mol/m^3.
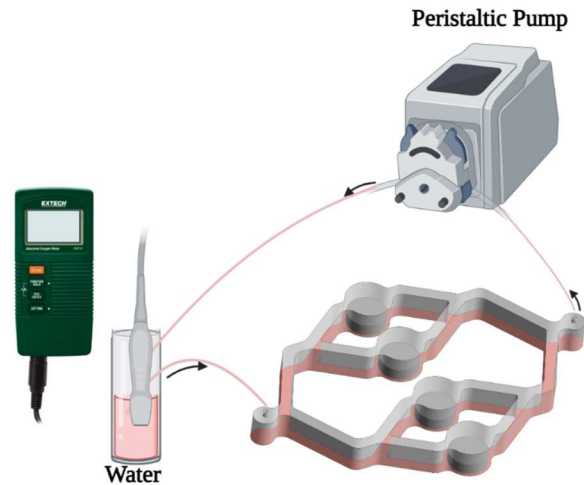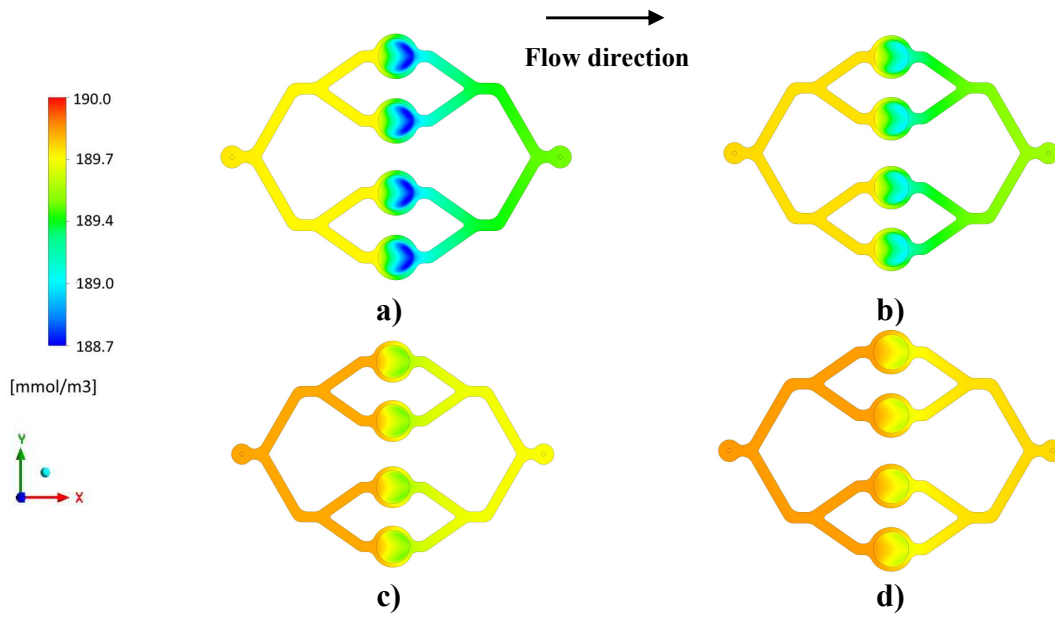
Figure 5. Scheme of the experimental setup used to measure the dissolved oxygen.

2.4 Numerical Solution

The governing equations were solved by using the commercial software Ansys® Fluent which applies the finite volume method. The first step consists of the domain discretization into control volumes and then the differential algebraic equations are discretized. The pressure equation was discretized by using the second-order scheme, the momentum equation by the second-order upwind scheme, and the first-order upwind scheme was used for the scalar. After obtaining the discretized equations, they were solved by using the Coupled scheme with a convergence criterion of 10^{-6} for all variables.
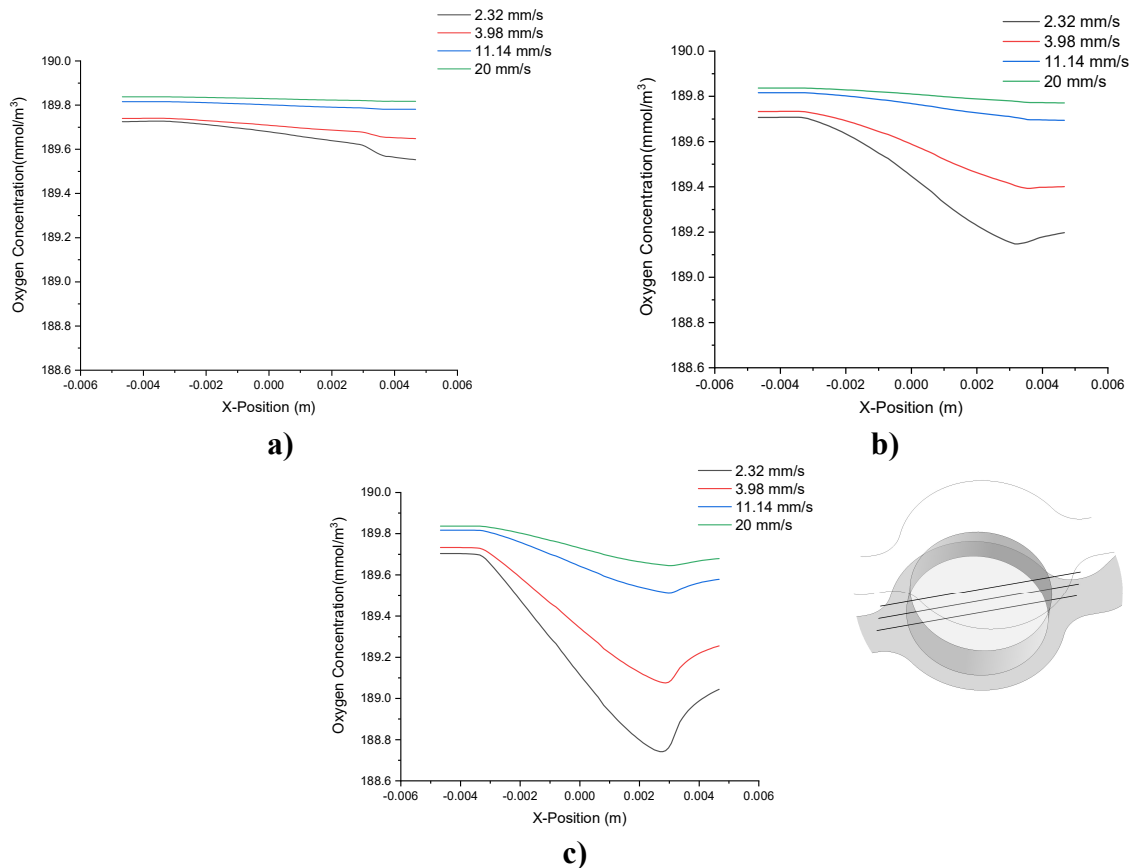
3   RESULTS AND DISCUSSION

Oxygen is an important factor in cell culture, and thus, in the present work, the oxygen distribution was evaluated when different velocities are imposed at the inlet. Figure 6 shows the contours of oxygen concentration for each velocity at the XY plane at z = 0. Looking at the results one can see that, before the organoids' region, the oxygen concentration is higher, and after them, the concentrations decreased due to their consumption by cells. Moreover, it can be seen that by increasing the velocity, the oxygen consumption is less evident since the number of cells considered in each organoid is the same and the oxygen concentration that reaches the organoids increases with the velocity increment. Consequently, the oxygen concentration that reaches the outlet is higher, and therefore a higher concentration enters the inlet. As previously mentioned, in the present work the recirculation of oxygen was considered which explains the high oxygen concentration from the inlet by increasing the velocity. Despite the previous differences, the oxygen gradient behavior is similar for all cases, showing a higher consumption in the final part of the organoid which is related to the fluid convection. Similar results were obtained by Lee et al. [24].

Figure 6. Oxygen concentration at the XY plane for a) v=2.32 mm/s, b) 3.98 mm/s, c) 11.14 mm/s and d) 20 mm/s.

To better observe the oxygen distribution along the device, three different heights (z = 2 mm, z = 1 mm, and z = 0 mm) were evaluated along the X-axis as plotted in Figure 7.
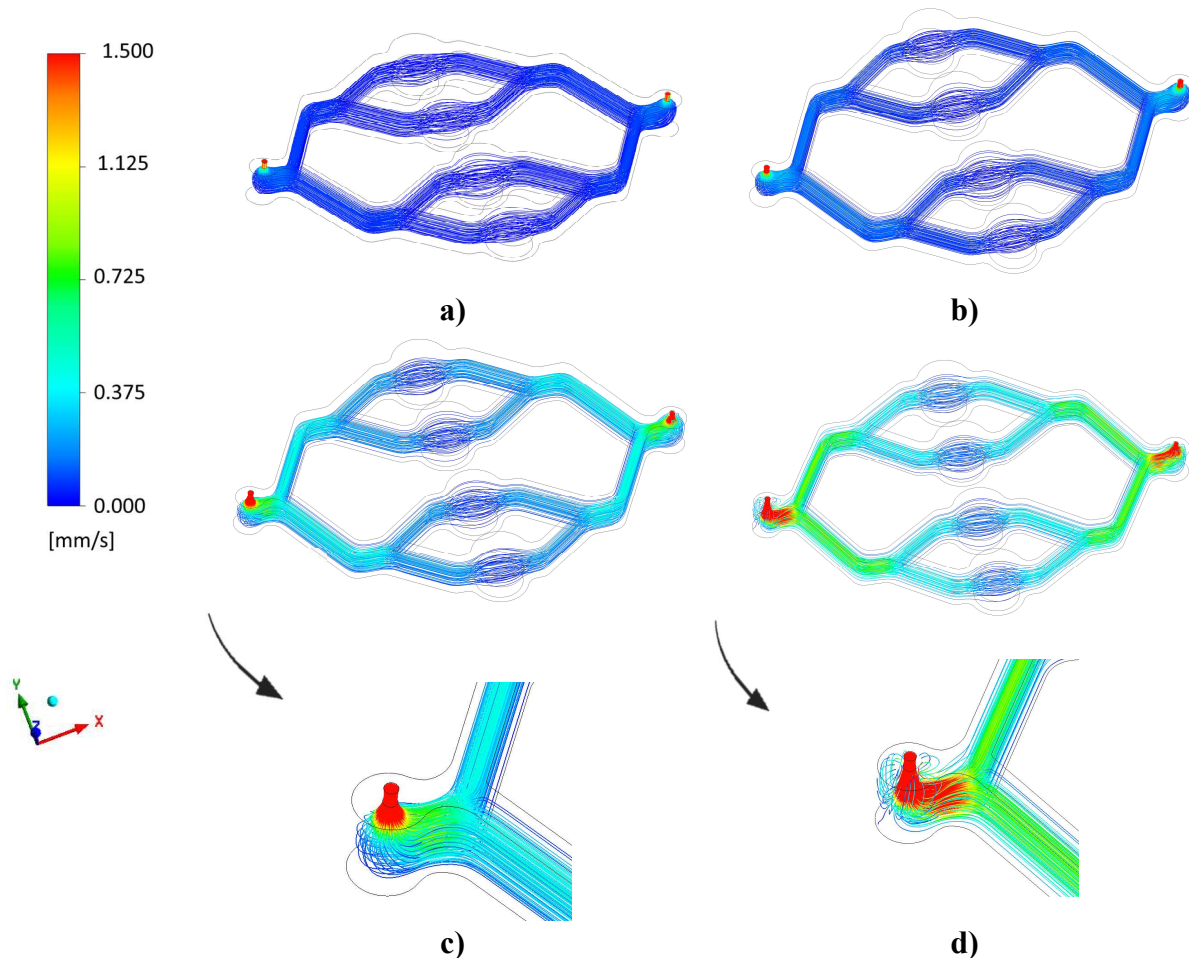

Figure 7. Oxygen concentration along the X-axis for each velocity at a) z = 2 mm, b), z = 1 mm, and c) z = 0 mm.

By analyzing these results, one can see that by increasing the inlet velocity, the oxygen concentration that reaches the organoids increase which supports the previous observations. Moreover, since the consumption rate is almost constant, the lower oxygen concentration is obtained with the lowest velocity.
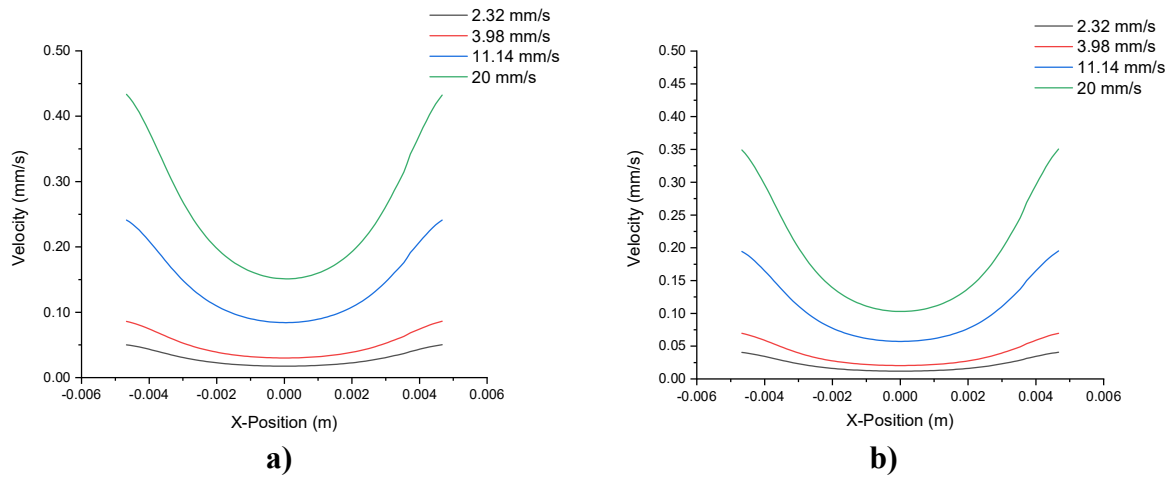
In order to observe the flow behavior inside the device, the velocity streamlines in the OoC were evaluated and the results are presented in Figure 8. Looking at the results one can see that higher velocities are attained at the inlet and outlet. Regarding the flow behavior, one can see that is similar in all cases, however, when the velocity is equal to 20 mm/s, recirculation zones are created at the inlet region. Although these are only observed at the fluid entrance is not intended to have these phenomena in this type of microfluidic device.

Figure 8. Velocity streamlines along the OoC for a) v=2.32 mm/s, b) 3.98 mm/s, c) 11.14 mm/s and d) 20 mm/s.

Since the previous results do not show the differences in the velocity magnitude in the organoid region, this was evaluated at the top and middle heights along the X-axis as depicted in Figure 9. As expected, the velocities at the organoid increase by increasing the inlet velocity but the velocity profiles are quite similar. Furthermore, the highest velocities' magnitudes are observed at the top of the organoid.

Figure 9. Velocity along the x-axis at a) z = 2 mm, b) z = 1 mm.

4   CONCLUSIONS

In the present work, numerical simulations were carried out in an organ-on-a-chip model comprising four channels in parallel to evaluate the effect of the inlet velocity on the oxygen distribution along the device. The results showed that the oxygen diffusion in the OoC was enhanced by the velocity increase. However, for the highest tested velocity (20 mm/s), it was observed the creation of vortices at the inlet region. These flow observations are important for future considerations in experimental tests and as a result, the numerical simulations proved to be a powerful tool to rapidly obtain a better understanding of the fluid flow and oxygen transport through the tested OoC and consequently improve the performance of this device.

5   ACKNOWLEDGMENTS

6   REFERENCES

[1]   D.Y. Park, J. Lee, J.J. Chung, Y. Jung, S.H. Kim, Integrating Organs-on-Chips:

Multiplexing, Scaling, Vascularization, and Innervation, Trends Biotechnol. 38 (2020) 99–112. https://doi.org/10.1016/j.tibtech.2019.06.006.

[2]   V. Carvalho, R.O. Rodrigues, R.A. Lima, S. Teixeira, Computational Simulations in Advanced Microfluidic Devices: A Review, Micromachines. 12 (2021) 1149. https://doi.org/10.3390/mi12101149.

[3]   V. Carvalho, M. Banobre, G. Minas, S. Teixeira, R.A. Lima, R.O. Rodrigues, The integration of spheroids and organoids into organ-on-a-chip platforms for tumour research : A review, Bioprinting. 27 (2022) e00224. https://doi.org/10.1016/j.bprint.2022.e00224.

[4]   I. Maia, V. Carvalho, R.O. Rodrigues, D. Pinho, S. Teixeira, A. Moita, T. Hori, H. Kaji, R.A. Lima, G. Minas, Organ-on-a-Chip Platforms for Drug Screening and Delivery in Tumor Cells: A Systematic Review, Cancers (Basel). 14 (2022) 1–25. https://doi.org/https://doi.org/ 10.3390/cancers14040935.

[5]   N. Filipovic, M. Nikolic, T. Sustersic, Simulation of organ-on-a-chip systems, in: N.E. Vrana, H. Knopf-Marques, J.B.T.-B. for O. and T.R. Barthes (Eds.), Woodhead Publ. Ser. Biomater., First, Woodhead Publishing, 2020: pp. 753–790. https://doi.org/https://doi.org/10.1016/B978-0-08-102906-0.00028-3.

[6]   V. Carvalho, I.M. Gonçalves, T. Lage, R.O. Rodrigues, G. Minas, S.F.C.F. Teixeira, A.S. Moita, T. Hori, H. Kaji, R.A. Lima, 3D Printing Techniques and Their Applications to Organ-on-a-Chip Platforms : A Systematic Review, Sensors. 21 (2021) 3304. https://doi.org/https://doi.org/10.3390/ s21093304.

[7]   K.-C.K.-C. Weng, Y.K. Kurokawa, B.S. Hajek, J.A. Paladin, V.S. Shirure, S.C. George, Human Induced Pluripotent Stem-Cardiac-Endothelial-Tumor-on-a-Chip to Assess Anticancer Efficacy and Cardiotoxicity, Tissue Eng. - Part C Methods. 26 (2020) 44–55. https://doi.org/10.1089/ten.tec.2019.0248.

[8]   J. Hübner, M. Raschke, I. Rütschle, S. Gräßle, T. Hasenberg, K. Schirrmann, A. Lorenz, S. Schnurre, R. Lauster, I. Maschmeyer, T. Steger-Hartmann, U. Marx, Simultaneous evaluation of anti-EGFR-induced tumour and adverse skin effects in a microfluidic human 3D co-culture model, Sci. Rep. 8 (2018) 15010. https://doi.org/10.1038/s41598-018-33462-3.

[9]   A. Zuchowska, A. Buta, B. Dabrowski, E. Jastrzebska, K. Zukowski, Z. Brzozka, 3D and 2D cell models in a novel microfluidic tool for evaluation of highly chemically and microbiologically pure graphene oxide (GO) as an effective drug carrier, Sensors Actuators, B Chem. 302 (2020) 127064. https://doi.org/10.1016/j.snb.2019.127064.

[10]   W. Shin, C.D. Hinojosa, D.E. Ingber, H.J. Kim, Human Intestinal Morphogenesis Controlled by Transepithelial Morphogen Gradient and Flow-Dependent Physical Cues in a Microengineered Gut-on-a-Chip, IScience. 15 (2019) 391–406. https://doi.org/10.1016/j.isci.2019.04.037.

[11]   V. Carvalho, N. Rodrigues, R.O. Rodrigues, R.A. Lima, S. Teixeira, Computational Analysis of Oxygen Transport in a Liver-on-a-chip platform, in: 7th Therm. Fluids Eng. Conf., 2022. https://doi.org/10.1615/TFEC2022.bio-ii.040844.

[12]   G.C. Kocal, S. Güven, K. Foygel, A. Goldman, P. Chen, S. Sengupta, R. Paulmurugan, Y. Baskin, U. Demirci, Dynamic Microenvironment Induces Phenotypic Plasticity of Esophageal Cancer Cells under Flow, Sci. Rep. 6 (2016) 1–11. https://doi.org/10.1038/srep38221.

[13] B. Zahorodny-Burke, B. Nearingburg, A.. Elias, Finite element analysis of oxygen transport in microfluidic cell culture devices with varying channel architectures , perfusion rates , and materials, Chem. Eng. Sci. 66 (2011) 6244–6253. https://doi.org/10.1016/j.ces.2011.09.007.

[14] B. Mosavati, A. V Oleinikov, E. Du, Development of an Organ-on-a-Chip-Device for Study of Placental Pathologies, Int. J. Mol. Sci. Artic. 21 (2020) 8755. https://doi.org/10.3390/ijms21228755.

[15] J.F. Wong, E.W.K. Young, C.A. Simmons, Computational analysis of integrated biosensing and shear flow in a microfluidic vascular model, AIP Adv. 7 (2017) 115116. https://doi.org/10.1063/1.5006655.

[16] S. Chen, J. Xue, J. Hu, Q. Ding, L. Zhou, S. Feng, Y. Cui, S. Lü, M. Long, Flow field analyses of a porous membrane-separated, double-layered microfluidic chip for cell co-culture, Acta Mech. Sin. 36 (2020) 754–767. https://doi.org/10.1007/s10409-020-00953-4.

[17] G. Hu, D. Li, Three-dimensional modeling of transport of nutrients for multicellular tumor spheroid culture in a microchannel, Biomed. Microdevices. 9 (2007) 315–323. https://doi.org/10.1007/s10544-006-9035-1.

[18] N.S. Bhise, V. Manoharan, S. Massa, A. Tamayol, M. Ghaderi, A liver-on-a-chip platform with bioprinted hepatic spheroids, Biofabrication. 8 (2016) 014101. https://doi.org/10.1088/1758-5090/8/1/014101.

[19] H.G.H.-G. Yi, Y.H. Jeong, Y. Kim, Y.J.Y.-J. Choi, H.E. Moon, S.H. Park, K.S. Kang, M. Bae, J. Jang, H. Youn, S.H. Paek, D.W.D.-W.D.W. Cho, A bioprinted human-glioblastoma-on-a-chip for the identification of patient-specific responses to chemoradiotherapy, Nat. Biomed. Eng. 3 (2019) 509–519. https://doi.org/10.1038/s41551-019-0363-x.

[20] I. Ansys, ANSYS® Fluent Theory Guide, Release 2020 R2, (2020).

[21] C. Poon, Measuring the density and viscosity of culture media for optimized computational fluid dynamics analysis of in vitro devices, BioRxiv. (2020). https://doi.org/10.1101/2020.08.25.266221.

[22] S.A.M. van Stroe-Biezen, F.M. Everaerts, L.J.J. Janssen, R.A. Tacken, Diffusion coefficients of oxygen, hydrogen peroxide and glucose in a hydrogel, Anal. Chim. Acta. 273 (1993) 553–560. https://doi.org/https://doi.org/10.1016/0003-2670(93)80202-V.

[23] D.A. Brown, W.R. MacLellan, H. Laks, J. C.Y. Dunn, B. M. Wu, R.E. Beygui, Analysis of oxygen transport in a diffusion-limited model of engineered heart tissue, Biotechnol. Bioeng. 97 (2007) 962–975. https://doi.org/https://doi.org/10.1002/bit.21295.

[24] J. Lee, S. Mehrotra, E. Zare-Eelanjegh, R.O. Rodrigues, A. Akbarinejad, D. Ge, L. Amato, K. Kiaee, Y.C. Fang, A. Rosenkranz, W. Keung, B.B. Mandal, R.A. Li, T. Zhang, H.Y. Lee, M.R. Dokmeci, Y.S. Zhang, A. Khademhosseini, S.R. Shin, A Heart-Breast Cancer-on-a-Chip Platform for Disease Modeling and Monitoring of Cardiotoxicity Induced by Cancer Chemotherapy, Small. 17 (2021). https://doi.org/10.1002/smll.202004258.